

Enhanced Photoelectrocatalytic Degradation Activity of Titanium Dioxide Photoelectrode: Effect of Film Thickness

N. A. Narewadikar^a, R. D. Suryavanshi^a, and K. Y. Rajpure^{a,*}

^aElectrochemical Materials Laboratory, Department of Physics, Shivaji University, Kolhapur, 416004 India

*e-mail: rajpure@yahoo.com

Received June 6, 2020; revised June 16, 2020; accepted July 3, 2020

Abstract—The present work reports the synthesis of titanium dioxide (TiO_2) thin films deposited from ethanolic titanium diisopropoxide bis-acetyl acetone precursor solution by using spray pyrolysis technique. The deposition of films were carried out on both amorphous and fluorine doped tin oxide (F:SnO_2) glasses. The effect of film thickness on photoelectrochemical, structural, morphological and optical properties of TiO_2 thin films was studied. The photoelectrochemical performance showed highest short circuit current and open circuit voltage at the optimized thickness of the film of $0.921\ \mu\text{m}$. X-ray diffraction study revealed that the films are polycrystalline, and exhibit anatase phase having tetragonal crystal structure. The TiO_2 electrodes deposited on fluorine-doped substrates were further used in the photoelectrochemical degradation of pollutants such as Methylene blue dye and benzoic acid. The degradation efficiencies were found to be 76 and 55% for the dye and benzoic acid, respectively.

DOI: 10.1134/S1061933X21010099

1. INTRODUCTION

Photodegradation of organic pollutants using immobilized photocatalysts is useful for limiting water pollution [1]. Currently, the metal oxide semiconductors such as TiO_2 [2], ZnO , Fe_2O_3 , CeO_2 , and SnO_2 are most frequently used to degrade various harmful organic pollutants such as dyes [3] via photocatalytic oxidation. Among the various metal oxide semiconductors, titanium dioxide (TiO_2) is one of the most attractive photocatalytic material due to its high efficiency, highly oxidizing photo-generated holes, high stability in a wide pH range and robustness to various irradiation wavelengths [4]. Since the pioneering work done by Fujishima and Honda [5], titanium dioxide has been recognized as one of most promising wide band gap semiconducting materials for the photocatalytic reactions as well as in photovoltaic devices such as dye-sensitized solar cells, lithium ion batteries [6] and perovskites solar cells [7].

Moreover, due to the wide band gap ($\sim 3.2\ \text{eV}$) of TiO_2 and its optical absorption in the ultraviolet region, researchers had made efforts to increase the photoelectrocatalytic (PEC) performance by examining synergistic effect of different synthesis parameters to harness more visible light.

Although there are many reports in the literature on various methods for the preparation of thin films of TiO_2 , spray pyrolysis remains the best technique due to its potential scalability in combination with the high adherence, uniformity, and transparency of the coat-

ings. The technique is quite simple and gives robust films [8]. There have been numerous publications studying the effect of film thickness on the photocatalytic behavior of TiO_2 where films were prepared by different techniques other than spray pyrolysis [9–12]. Wang et al. [13] reported surface-mediated method to grow transparent and oriented anatase TiO_2 films with tunable, well defined nanocrystalline morphologies to analyze the structure-dependent physical and chemical properties, and for improving the performance of the material and devices. Ayouchi et al. [14] presented the growth and characterization of TiO_2 thin films on p-Si(100) and fused silica substrates by chemical spray pyrolysis. Choi et al. [15] synthesized highly porous and hydrophilic nanostructured TiO_2 thin films and particles by sol-gel method for significant improvement of the photocatalytic activity of the films mainly due to their high surface area and porosity. The films were applied as highly efficient photocatalysts to decolorize Methylene blue (MB) dye.

This work describes the formation and characterization of anatase TiO_2 thin films by chemical spray pyrolysis and their applications in the dye degradation. An attempt is made to intensify the PEC performance of TiO_2 photoelectrode by varying film thickness and by developing more ordered crystalline structure on conducting substrates. To test the PEC behavior of the thin film electrodes two model pollutants, MB and benzoic acid (BA), were used. A comparative analysis of the results was applied to optimize thickness of the

film to achieve the best efficiency of the photoelectrode.

2. EXPERIMENTAL SECTION

2.1. Materials

All chemicals used for the deposition of TiO_2 thin films were of analytical grade. Titanium diisopropoxide bis-acetyl acetonate 75 wt % in propanol-2 (Sigma Aldrich) was used as Ti source. Ethanol (99.9% purity), fluorine doped tin oxide (FTO) ($15\text{--}20 \Omega/\square$ resistivity), Methylene blue and benzoic acid were purchased from SD Fine Chem. Ltd. All chemicals were used without further purification.

2.2. Material Characterization

The PEC performance was studied by using two-electrode cell system for measurement of short circuit current (I_{sc}) and open circuit voltage (V_{oc}). Bruker X-ray diffractometer Model D2 with CuK radiation of wavelength 1.5406 \AA was used for an identification of phases and structural analysis. FESEM and EDAX spectra were recorded by using scanning electron microscope (Oxford Instrument, model- MIRA 3 LMH). Absorption and transmission spectra of the films were recorded at room temperature by using a UV-visible spectrophotometer (Shimadzu). FT-Raman spectrum of film was measured within the wavenumber range of $100\text{--}700 \text{ cm}^{-1}$ using MultiRAM spectrometer (Bruker) with a He-Ne laser source with an excitation wavelength of 532 nm.

2.3. Preparation of TiO_2 thin Films

TiO_2 thin films on bare glass and FTO coated glass (with sheet resistance of $10\text{--}20 \Omega/\square$) were synthesized by spray pyrolysis technique using ethanolic solution of titanium diisopropoxide bis(acetyl acetonate) at low temperature (350°C) and subsequently annealed at 500°C for 1 h. The film thickness was controlled by varying the quantity of spraying solution within $40\text{--}70 \text{ mL}$ adding 10 m at each next step. The solution and carrier gas (compressed air) were fed into a spray nozzle at a pre-adjusted constant atomization [16] and sprayed at flow rate of $3 \text{ cm}^3 \text{ min}^{-1}$.

2.4. Photoelectrocatalytic Activity and Photodegradation Test

The PEC cell comprised two electrodes, in which the spray synthesized TiO_2 thin films on conducting FTO coated glass was used as a working electrode and platinum wire as a counter electrode. The 0.1 M NaOH solution was used as an electrolyte [17]. The distance between working and counter electrodes was kept 0.5 cm. An open circuit voltage (V_{oc}) and short circuit current (I_{sc}) of the cell were measured by illu-

minating photoelectrode with 20 W UV Omnilux lamp with an excitation wavelength of 365 nm. Large area ($10 \times 10 \text{ cm}^2$) photoelectrodes were prepared and tested in prototype PEC reactor employing a stainless steel as a counter-electrode and UV tube lamps with $\lambda = 320$ and 400 nm .

The degradation of MB and BA model pollutants was studied at external bias potential (1.5 V) in the presence of TiO_2 photoelectrode. To provide water recirculation through PEC cell equipped with silicon tubes, the Ravel peristaltic pump was applied at a constant flow rate [18]. During the adsorption/desorption processes, liquid samples were collected at regular time intervals every 40 min and were used for further analysis. The concentration of the pollutants in the solution was determined by measuring the extinction spectra recorded using UV-visible spectrophotometer. The degradation percentage (D) was calculated using the equation reported elsewhere [16]. Chemical oxygen demand (COD) on the same samples was measured using the standard method of oxidation with an excess amount of potassium dichromate (strong oxidizing agent) in concentrated sulfuric acid after digestion at 125°C for 2 hours.

3. RESULTS AND DISCUSSION

3.1. Photoelectrochemical (PEC) Analysis

In this work, four films with a thickness varied from 0.720 to $1.370 \mu\text{m}$ were prepared by spray pyrolysis technique. The variations of short circuit current (I_{sc}) and open circuit voltage (V_{oc}) with respect to the amount of solution of TiO_2 spread onto the photoelectrode under UV-light irradiation are shown in Fig. 1.

The values of I_{sc} and V_{oc} gradually increase with the thickness of the films and then decrease sharply for thick films due to the poor adhesion. The film with $0.921 \mu\text{m}$ thickness shows maximum values ($I_{sc} = 953 \mu\text{A}$ and $V_{oc} = 0.980 \text{ V}$) and it acts as an efficient catalyst due to the fast migration of the photogenerated charge carriers. The value of PEC efficiency depends on various factors such as crystallinity of the material, thickness and optical properties of the film. The magnitude of the open circuit voltage increases with the negative polarity towards the TiO_2 photoelectrode [19], suggesting that the deposited TiO_2 film exhibits n-type conductivity. The main contribution of the TiO_2 electrode to the photocurrent has a PEC origin as evidenced by the fast charge transfer kinetics. The observed maximal photocurrent $I_{sc} = 953 \mu\text{A}$ for bare TiO_2 is comparatively higher than the previously reported values [20–24]. For instance, Feng et al. [25] reported the synthesis of highly ordered, multi-layered, continuous mesoporous TiO_2 thin films with photocurrent density $J_{sc} = 0.35 \text{ mA cm}^{-2}$. Rahman and his co-workers [26] described TiO_2 nanoflowers synthesized by the phase liquid deposition technique

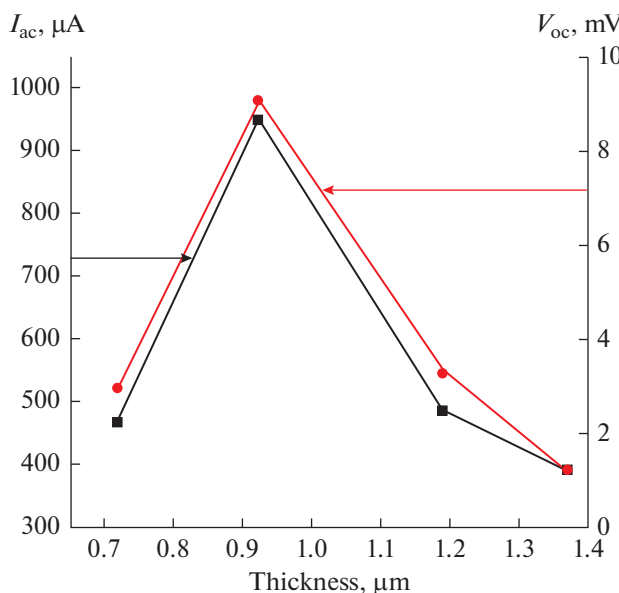


Fig. 1. The variation of J_{sc} and V_{oc} of a PEC cell with configuration n-TiO₂/0.1 M NaOH/Pt as a function of film thickness for the spray deposited TiO₂ thin film under UV illumination.

assisted with a polyvinylpyrrolidone and showed that $J_{sc} = 0.068 \text{ mA cm}^{-2}$ at 0.36 V. Pu et al. [27] reported the deposited TiO₂ nanowires with observed current density of 0.82 mA cm^{-2} .

3.2. X-ray Diffraction Study

XRD patterns of the TiO₂ thin films with different thickness are shown in Fig. 2. The films exhibit polycrystalline structure. The TiO₂ is present in anatase phase (Standard JCPDS cards nos. 84-1286, 71-1167, 86-1157). As the film thickness increases up to 920 nm of thickness, the crystallinity increases accordingly. The decrease in crystallinity after 920 nm thickness might be due to formation of powdery films formed with 60 MMM. At this quantity, provided substrate temperature (350°C) must have been insufficient for a complete decomposition of the substrate and crystallization of the films. Based on Debye–Scherrer equation, an average crystallite size of optimized TiO₂ film along most preferred (101) plane was calculated to be 26 nm as shown in Table 1 [28].

3.3. FESEM with EDX Analysis

Surface morphology and compositional analysis of TiO₂ films deposited at various thicknesses were studied by FESEM with EDX techniques. Figure 3a shows the FESEM image of the TiO₂ film with a thickness 0.92 μm. The metal oxide particles are closely packed into porous structure with high roughness providing better photocatalytic performance. The EDX spec-

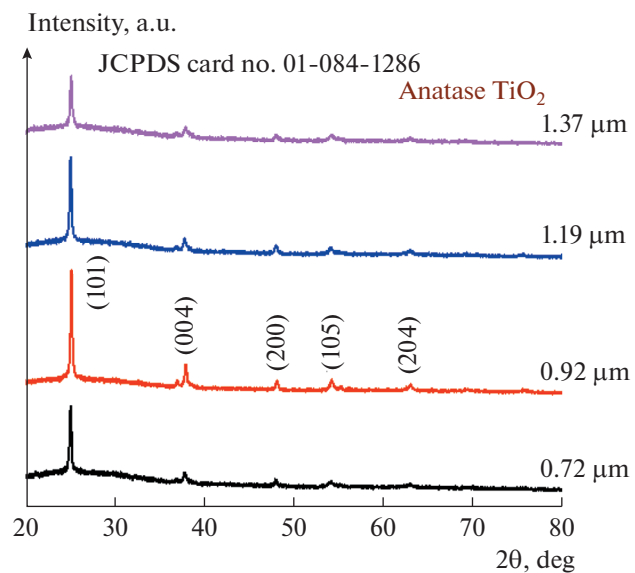


Fig. 2. XRD patterns of anatase TiO₂ thin film with different thickness.

trum of TiO₂ reveals uniform distribution of Ti and O on the surface; the peaks with less intensity correspond to Si element (Fig. 3b). The data suggest that the deposited films possess sub-stoichiometric composition. The elemental atomic percentages determined by EDX analysis were 29.26% for Ti and 70.74% for O, respectively.

3.4. Optical Studies

The Fig. 4a shows the absorption spectra of the spray deposited TiO₂ thin films. The band gap energy (E_g) of the deposited films was obtained by analyzing the optical data using the expression given in [29]. It shows that TiO₂ absorbs in the ultraviolet region. The Taut plot gives the range of the band gap values from 3.29 to 3.21 eV as shown in the inset in Fig. 4a.

Table 1. Calculated values of thickness, band gap and crystallite size of the prepared samples

No.	Thickness, μm	Band gap, eV	Crystallite size, nm
1	0.72	3.29	26
2	0.92	3.27	26
3	1.19	3.24	33
4	1.37	3.21	32

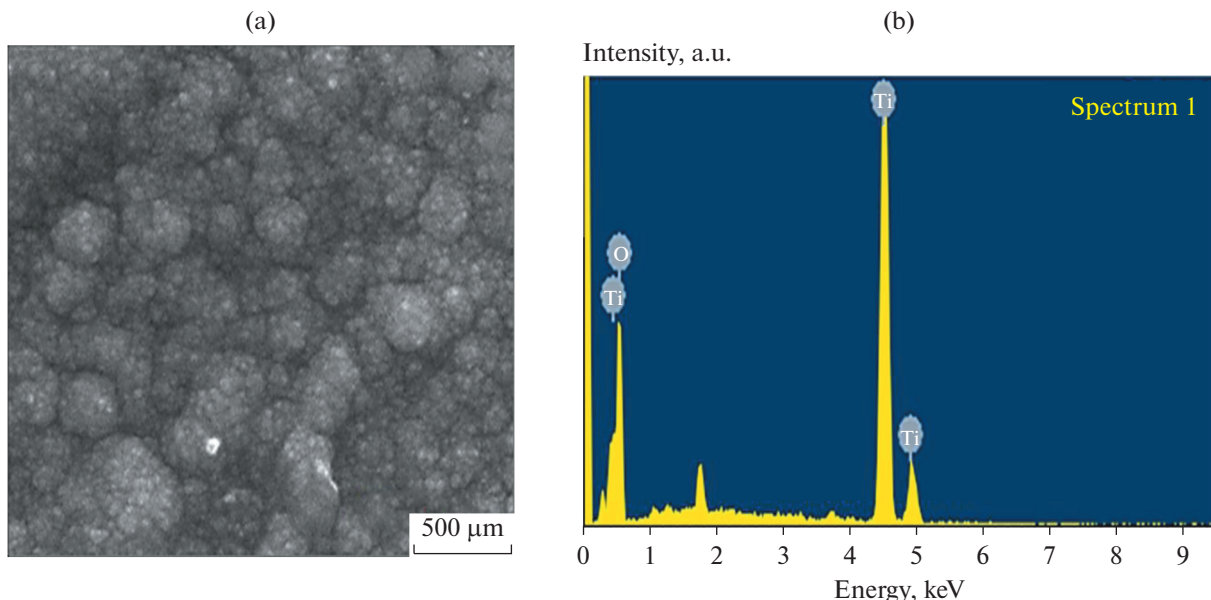


Fig. 3. (a) FESEM image and (b) EDX spectrum of TiO_2 thin film with a thickness $0.92 \mu\text{m}$.

The results are in agreement with reported values [30]. Figure 4b shows the transmittance spectra of the TiO_2 thin films. The transparency of the films decreases with its thickness. The transmittance spectra exhibit the interference patterns suggesting high reflectance and scattering. The numbers of minima or maxima within the studied range of wavelength are around 10 that corresponds to a micrometer thickness. Optimized film is transparent by 72% at $\lambda = 365 \text{ nm}$. The thickness, band gap and crystallite size are summarized in Table 1. Figure 5 shows the change of thickness depending on the crystallite size of TiO_2 .

3.5. Raman Spectroscopy

Raman spectroscopy was applied to evaluate the structural disorder of the different oxides used herein. A typical Raman spectrum of the TiO_2 thin film deposited at optimized conditions is shown in Fig. 6. The sample showed the well-known Raman bands for anatase TiO_2 [31]: the most intense E_g mode at 144 cm^{-1} , and the other three B_{1g} , A_{1g} and E_g modes at 398 , 517 and 640 cm^{-1} , respectively. A small peak at 197 cm^{-1} is assigned to the other E_g frequency mode appearing due to intrinsically weak vibrations in anatase TiO_2 . These results correlate well with the previously reported data [29].

In perfect infinite crystal, inelastic scattering of incident radiation is contributed by only phonons close to the center of the Brillouin zone (BZ). When crystal size is of the nanometer scale, a larger portion of the BZ is allowed to participate in scattering pro-

cesses. Therefore, small changes in the Raman frequency peaks of the Raman band can be observed. According to the phonon dispersion curve of anatase TiO_2 , the spectrum of the TiO_2 film in Fig. 6 represents the main peak of the E_g mode at 141 cm^{-1} [32, 33].

3.6. Photoelectrocatalytic Degradation

The efficient photocatalytic degradation of organic pollutants over TiO_2 photocatalysts are generally attributed to the strong oxidizing ability of highly reactive species such as hydroxyl radicals. However, such species do not possess selectivity because the surface of TiO_2 is negatively charged after NaOH modification, which is beneficial for the non-selective adsorption [34]. The PEC performance of TiO_2 photoelectrode was studied for the degradation of both MB and BA using the single cell PEC reactor under UV light irradiation. In the control experiments, the pollutants did not undergo degradation under direct UV illumination in the absence of the photocatalyst. There was a slight decrease of extinctions of MB and BA; this may be due to the adsorption loss of electrolyte through circulation pipes and degradation reactor when degradation is carried out with TiO_2 photocatalyst without UV irradiation. Therefore, both light and catalyst are required for an effective degradation of an organic pollutant.

The aqueous solutions of model pollutants with concentration of 1 mM were re-circulated with a constant flow rate. The probes were taken every 40 min for

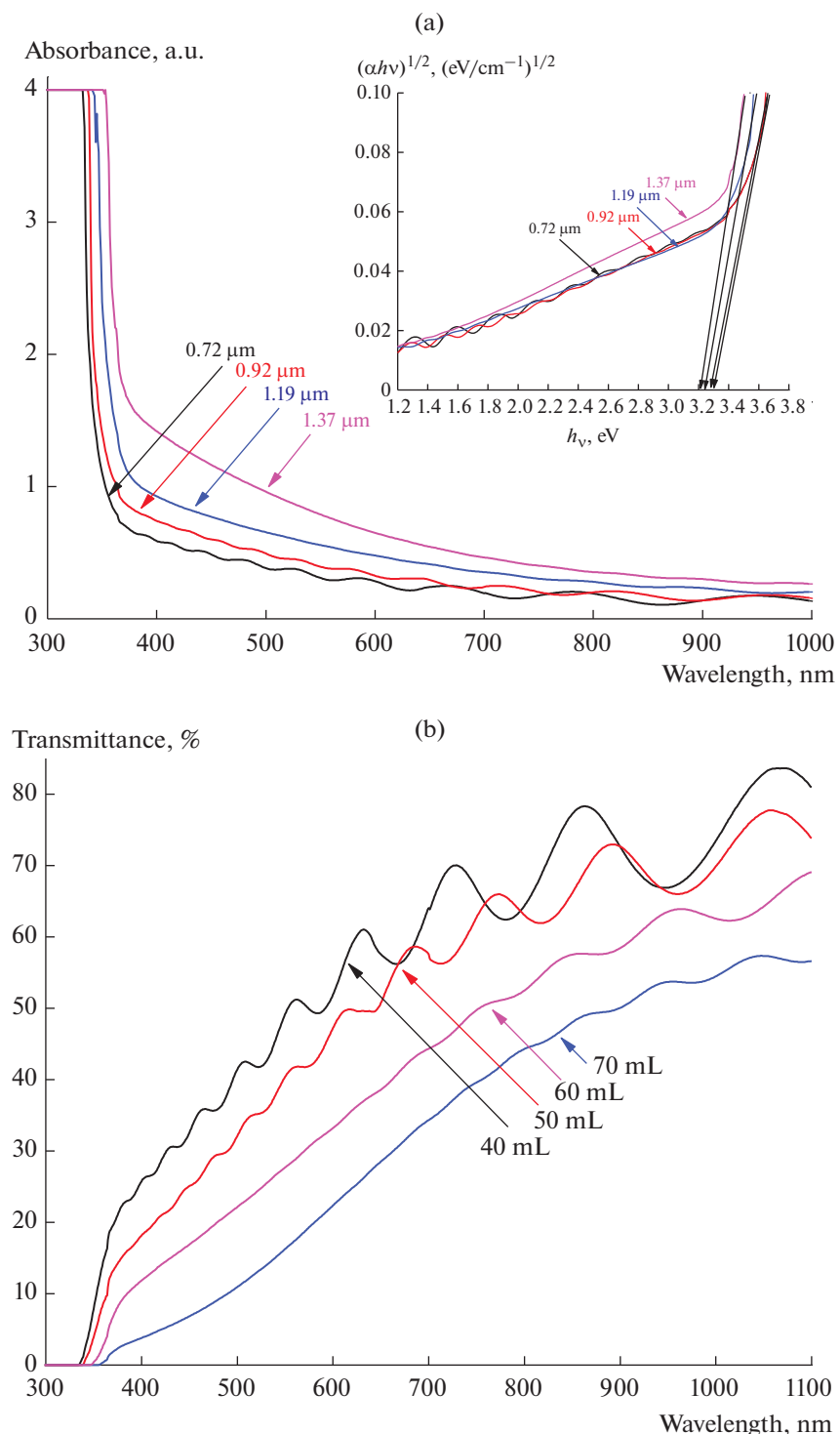


Fig. 4. (a) Optical absorbance and (b) transmittance spectra of TiO_2 thin films with different thickness.

within 320 min for MB and 300 min for BA, respectively.

The degradation performances were studied by calculating degradation percentage D using the equation from [35]. The results are shown in Table 2.

The concentrations of both MB and BA decreased with time due to their decomposition. Figure 7a–d show the PEC degradation of MB and BA using TiO_2 photoanode under UV illumination. Figure 7b,d show the changes in the extinction spectra of MB and BA, collected at various intervals during photocatalytic

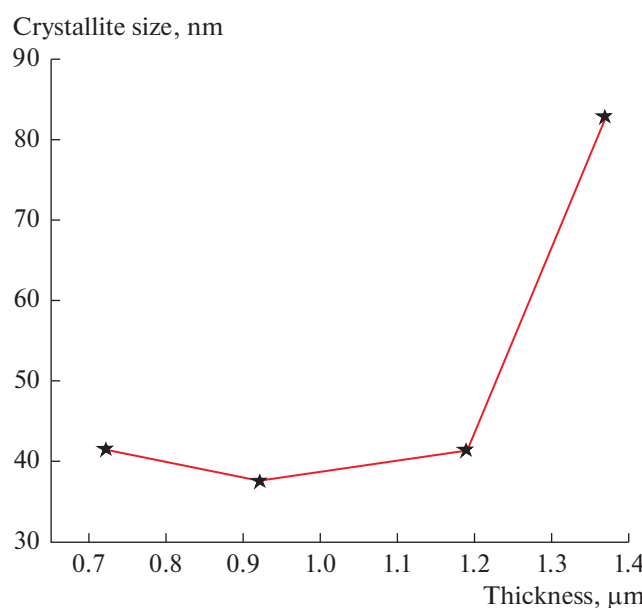


Fig. 5. Dependence of crystallite size vs thickness of the TiO_2 films.

degradation recorded in the wavelength range from 400 to 850 nm. The insets in Fig. 7b, d show the time dependencies of degradation efficiency. The photo-catalytic degradation follows a pseudo first order reaction and its kinetics can be expressed using the equation given in [36]. The data points were fitted linearly as shown in Fig. 7a, c to calculate the apparent rate constant and the MB and BA degradation rates per gram of photocatalyst ($1.5 \times 10^{-4} \text{ s}^{-1}$ and $1 \times 10^{-3} \text{ s}^{-1}$), respectively.

Here, decomposition of pollutants occurs through generating the charge carriers under UV illumination on the photoelectrode surface. The generated electrons travel through an external circuit towards the counter electrode. The holes left behind in valence band come on the semiconductor surface towards an electrolyte which model organic species MB and BA to produce hydroxyl radical $\text{OH}\cdot$, which acts as a strong oxidation agent [37].

The degradation kinetics is calculated at maximal absorption of MB and BA at 661 and 231 nm, respectively. The degradation efficiency values for MB dye

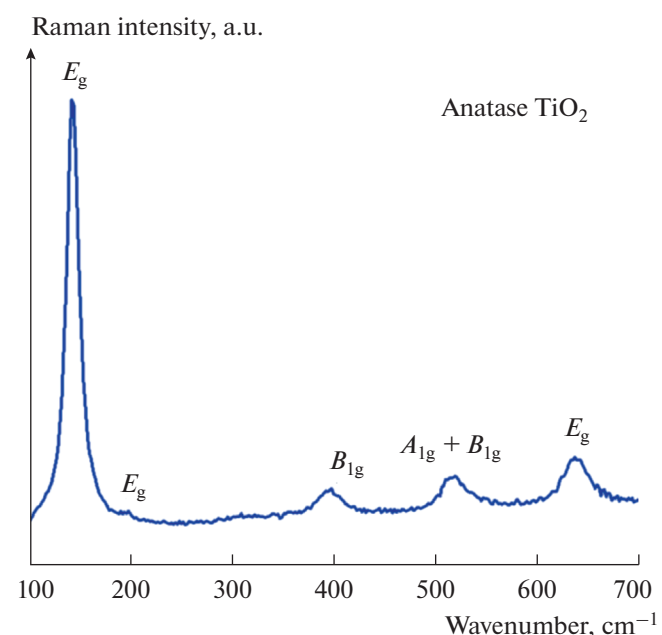


Fig. 6. Raman spectrum of the spray deposited TiO_2 thin film with a thickness 0.92 μm .

and BA (76 and 55%, respectively) are higher than those reported earlier [38]. Figure 7a,b show the degradation kinetics of MB and BA on TiO_2 photocatalysts. The kinetics follows the Langmuir–Hinshelwood first-order model and obeys the pseudo-first order kinetics equation [39].

Figure 8 depicts the variation in chemical oxygen demand (COD) in the course of time using TiO_2 photoelectrodes. The COD was measured by titration method to obtain more accurate results. This study provides information about the concentration of oxidizable matter left in the electrolyte solution. The process completed within 120 min at 125°C in COD analyzer. The COD values decrease with time. The rate of mineralization changes slowly in the initial period and then started to decrease rapidly. This decreased rate indicates the formation of by-products, which has a low reaction rate with hydroxyl radicals. COD values decreases from 60 to 25 mg L^{-1} and 72 to 18 mg L^{-1} with reaction time for MB and BA, respectively. The COD values show mineralization close to that of water standard (10 mg L^{-1}).

CONCLUSIONS

The polycrystalline TiO_2 thin films were successfully deposited by the spray pyrolysis technique at reasonably low temperature. The results showed that relatively highest values of I_{sc} and V_{oc} can be obtained at 0.921 μm thickness of TiO_2 thin film. X-ray diffraction analysis revealed that the TiO_2 thin films possess tetragonal structure with pure anatase phase which

Table 2. Kinetic parameters and values of degradation of MB and BA using TiO_2 photoelectrode

Pollutant	k, s^{-1}	Degradation, %
Methylene blue	0.00157	76 (320 min)
Benzoic acid	0.001	55 (300 min)

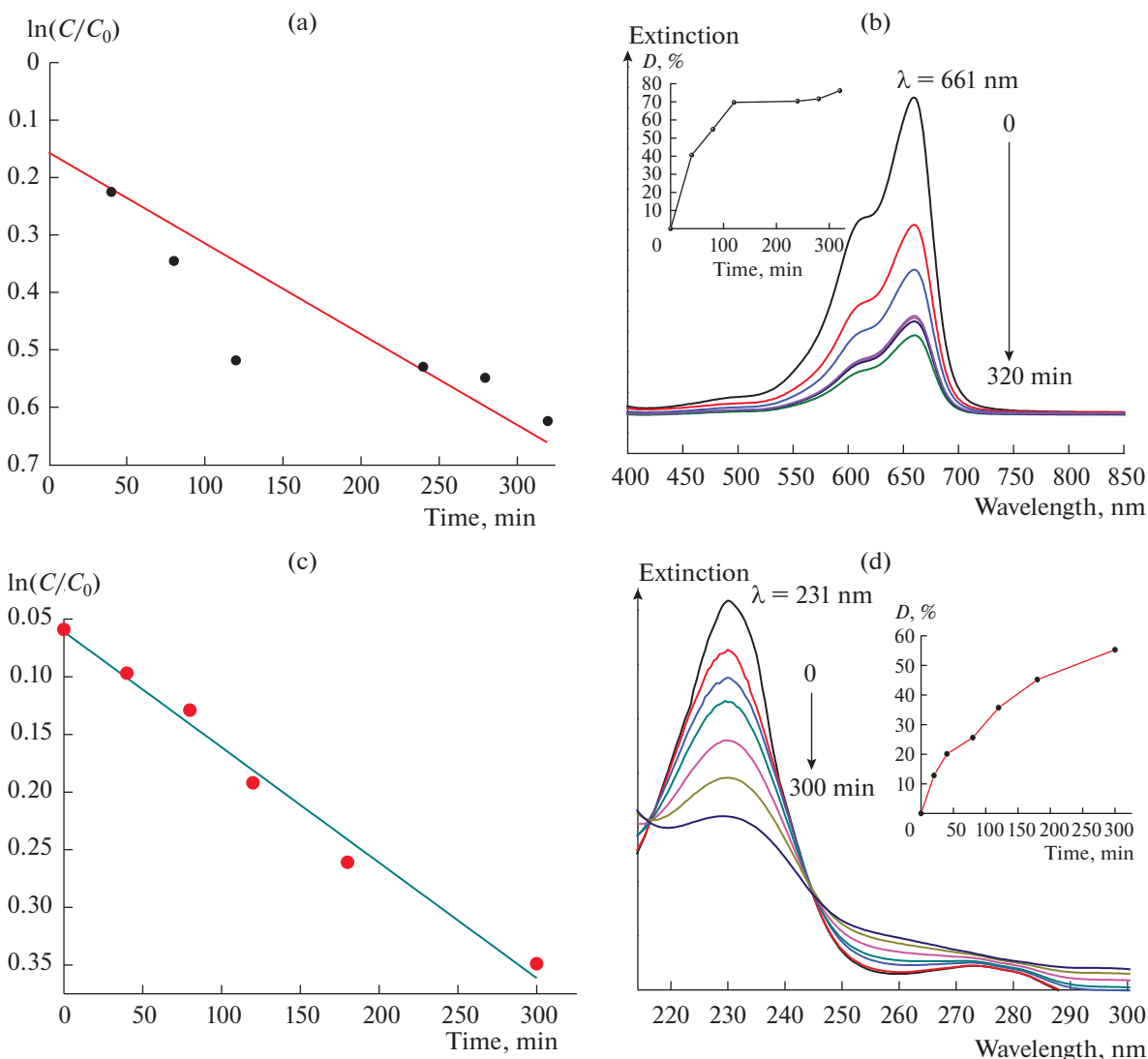


Fig. 7. Degradation of MB and BA on TiO_2 under UV illumination: (a) kinetics of degradation of MB (extinction taken at 661 nm); (b) corresponding extinction spectra for different reaction times; (c) kinetics of degradation of BA (extinction taken at 231 nm); and (d) extinction spectra for different reaction time.

was further confirmed by Raman analysis. The FESEM micrograph showed compact surface morphology of the film while EDX analysis revealed the presence of Ti and O elements. The PEC degradation values of MB and BA were 76 and 55%, respectively. The COD values demonstrated the extent of mineralization of both MB and BA. Therefore, it is concluded that the deposited film of thickness 0.921 μm showed better PEC performance for degradation of these organic pollutants. The results might be useful for obtaining thin film photoelectrodes with better performances from other photocatalytic materials by taking this optimal film thickness as a reference.

ACKNOWLEDGMENTS

The authors gratefully acknowledge the financial support received from Chhatrapati Shahu Maharaj Research Training and Human Development Institute (SARTHI), Pune (Government of Maharashtra) for the Chhatrapati Shahu Maharaj Senior Research Fellowship-(CMSRF) 2019, DST PURSE Phase-II (2018–2022) and UGC DSA Phase-II (2018–2023).

CONFLICT OF INTEREST

The authors declare that they have no conflicts of interest.

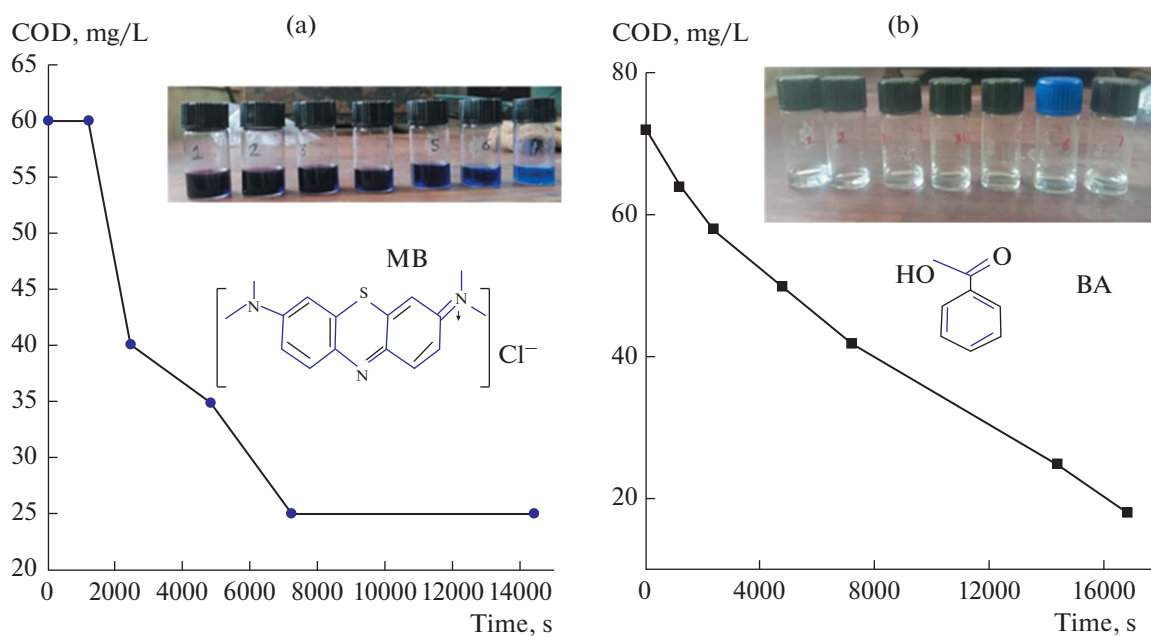


Fig. 8. The plot of COD vs reaction time for (a) MB dye and (b) BA.

REFERENCES

- Kusmierenk E., *Catalysts*, 2020, vol. 10, p. 439.
- Sampath, C., Ranasinghe, K., Vequizo, J.J.M., and Yamakata, A., *J. Photochem. Photobiol. A*, 2018, vol. 358, p. 320.
- Grätzel, M., *Nature*, 2001, vol. 414, p. 338.
- Linsebigler, A.L., Lu, G., and Yates, J.T., *Chem. Rev.*, 1995, vol. 95, p. 735.
- Chen, X. and Mao, S.S., *Chem. Rev.*, 2007, vol. 107, p. 2891.
- Bai, H., Liu, Z., and Sun, D.D., *J. Mater. Chem.*, 2012, vol. 22, p. 24552.
- Ma Y., Wang X., Jia Y., Chen X., Han H., and Can Li C., *Chem. Rev.*, 2014, vol. 114, p. 9987.
- Okuya, M., Nakade, K., and Kaneko, S., *Sol. Energy Mater. Sol. Cells*, 2002, vol. 70, p. 425.
- Tada, H. and Tanaka, M., *Langmuir*, 1997, vol. 13, p. 360.
- Regonini, D., Alves, A.K., Berutti, F.A., and Clemens, F., *Int. J. Photoenergy*, 2014, vol. 2014, 472539.
- Jung, S.C., Kim, S.J., Imaishi, N., and Cho, Y.I., *Appl. Catalysis B*, 2005, vol. 55, p. 253.
- Xianyu, W.X., Park, M.K., and Lee, W.I., *Korean J. Chem. Eng.*, 2001, vol. 18, p. 903.
- Wang, D., Liu, J., Huo, Q., Nie, Z., Lu, W., Williford, R.E., and Jiang, Y.-B., *J. Am. Chem. Soc.*, 2006, vol. 128, p. 13670.
- Ayouchi, R., Casteleiro, C., Schwarz, R., and Barrado, J.R., *Phys. Status Solidi C*, 2010, vol. 7, p. 933.
- Choi, H., Stathatos, E., and Dionysiou, D.D., *Thin Solid Films*, 2006, vol. 510, p. 107.
- Sapkal, R.T., Shinde S.S., Waghmode T.R., Govindwar S.P., Rajpure K.Y., and Bhosale C.H., *J. Photochem. Photobiol. B*, 2012, vol. 110, p. 15.
- Mohite, V.S., Mahadik, M.A., Kumbhar, S.S., Kothavale, V.P., Moholkar, A.V., Rajpure, K.Y., and Bhosale, C.H., *Ceram. Int.*, 2014, vol. 41, p. 2202.
- Suryavanshi, R.D., Mohite, S.V., Bagade, A.A., Shaikh, S.K., Thorat, J.B., and Rajpure, K.Y., *Mater. Res. Bull.*, 2018, vol. 101, p. 324.
- Duminica, F.D., Maury, F., and Abisset, S., *Thin Solid Films*, 2013, vol. 515, p. 7732.
- Kibasomba, P.M., Dhlamini, S., Maaza, M., Liu, C.P., Rashad, M.M., Rayan, D.A., and Mwakikunga, B.W., *Results Phys.*, 2018, vol. 9, p. 628.
- Shinde, P.S., Patil, P.S., Bhosale, P.N., and Bhosale, C.H., *J. Am. Ceram. Soc.*, 2008, vol. 91, p. 1266.
- Maulidiyah, M., Wijawan, I.B.P., Wibowo, D., Aladin, A., Hamzah, B., and Nurdin, M., *IOP Conf. Ser. Mater. Sci. Eng.*, 2018, vol. 367, 012060.
- Haro, M., Abargues, R., Herraiz-Cardona, I., Martínez-Pastor, J., and Giménez, S., *Electrochim. Acta*, 2014, vol. 144, p. 64.
- Yen, Y.C., Chen, J.A., Ou, S., Chen, Y.S., and Lin, K.J., *Sci. Rep.*, 2017, vol. 7, 42524.
- Wang, G., Yang, Y., Ling, Y., Wang, H., Lu, X., Pu, Y.C., Zhang, J.Z., Tong, Y., and Li, Y., *J. Mater. Chem. A*, 2016, vol. 4, p. 2849.
- Feng, D., Luo, W., Zhang, J., Xu, M., Zhang, R., Wu, H., Lv, Y., Asiri, A.M., Khan, S.B., Rahman, M.M., Zheng, G., and Zhao, D., *J. Mater. Chem. A*, 2013, vol. 1, p. 1591.
- Rahman, M.Y.A., Umar, A.A., Roza, L., and Salleh, M.M., *J. Exp. Nanosci.*, 2015, vol. 10, p. 925.

28. Pu, Y.C., Wang, G., Chang, K.D., Ling, Y., Lin, Y.K., Fitzmorris, B.C., Liu, C.M., Lu, X., Tong, Y., Zhang J.Z., Hsu, Y.J., and Li, Y., *Nano Lett.*, 2013, vol. 13, p. 3817.
29. Ezema, C.G., Nwanya, A.C., Ezema, B.E., Patil, B.H., and Bulakhe, R.N., Ukoha P.O., Lokhande, C.D., Maaza, M., and Ezema, F.I., *Appl. Phys. A*, 2016, vol. 122, 435.
30. Yang, Y., Xu, L., Wang, H., Wang, W., and Zhang, L., *Mater. Des. J.*, 2016, vol. 108, p. 632.
31. Balachandran, U. and Eror, N.G., *J. Solid State Chem.*, 1982, vol. 42, p. 276.
32. Stagi, L., Carbonaro, C.M., Corpino, R., Chiriu, D., and Ricci, P.C., *Phys. Status Solidi B*, 2015, vol. 252, p. 124.
33. Salis, M., Ricci, P.C., and Anedda, A., *J. Raman Spectrosc.*, 2009, vol. 40, p. 64.
34. Sajan, C.P., Wageh, S., Al-Ghamdi, A.A., and Yu, J., *Nano Res.*, 2016, vol. 9, p. 3.
35. Manikandan, A.S. and Renukadevi, K.B., *Mater. Res. Bull.*, 2017, vol. 94, p. 85.
36. Mahadik, M.A., Shinde, S.S., Pathan, H.M., Rajpure, K.Y., and Bhosale, C.H., *J. Photochem. Photobiol. B*, 2014, vol. 141, p. 315.
37. Shinde, S.S., Bhosale, C.H., and Rajpure, K.Y., *Catal. Rev. Sci. Eng.*, 2013, vol. 55, p. 79.
38. Mohite, V.S., Mahadik, M.A., Kumbhar, S.S., Hunge, Y.M., Kim, J.H., Moholkar, A.V., Rajpure K.Y., and Bhosale, C.H., *J. Photochem. Photobiol. B*, 2014, vol. 142, p. 204.
39. Mahadik, M.A., Shinde, S.S., Mohite, V.S., Kumbhar, S.S., Rajpure, K.Y., Moholkar, A.V., and Bhosale, C.H., *Ceram. Int.*, 2014, vol. 40, p. 9463.

SPELL: 1. OK